

We are IntechOpen, the world's leading publisher of Open Access books Built by scientists, for scientists

6,900

Open access books available

186,000

International authors and editors

200M

Downloads

Our authors are among the

154

Countries delivered to

TOP 1%

most cited scientists

12.2%

Contributors from top 500 universities



WEB OF SCIENCE™

Selection of our books indexed in the Book Citation Index
in Web of Science™ Core Collection (BKCI)

Interested in publishing with us?
Contact book.department@intechopen.com

Numbers displayed above are based on latest data collected.
For more information visit www.intechopen.com



Pressure sensing line diagnostics in nuclear power plants

Kang Lin and Keith E. Holbert
Arizona State University
U.S.A.

1. Introduction

Nuclear power plants (NPPs) have been designed to attain safe and reliable functioning through the monitoring and analysis of various critical operational parameters. Data obtained from monitoring systems provide for the control of feedwater flows, recirculation flows, reactor water levels, etc. and can be used to initiate emergency procedures, such as water injection into the reactor coolant system. Therefore, it is crucial for sensing equipment to precisely convey neutron flux, temperature, pressure, level, and flow of plant processes to assure the continued safe and reliable operation of a NPP.

A differential pressure transmitter is used to measure fluid flow and level while a non-differential transducer is utilized to measure absolute and gauge pressure. A NPP generally uses about 200 to 800 pressure and differential pressure sensors to measure the process pressure, level, and flow in its primary and secondary systems (Hashemian, 2006). Pressure transmitters are usually located away from the process to protect them from the adverse effects of ambient temperature, radiation, and vibration on the operability and qualified life of the sensor (Hashemian, 2006). For example, high ambient temperatures will have effects on the mechanical components of the transmitter and shorten the life of its electronics.

Pressure sensing lines, also referred to as impulse or instrument lines, are employed to couple a pressure transmitter to the process piping, reactor vessel, or primary flow elements to convey a pneumatic or hydraulic signal from the process to the sensors. In some industrial plants, the pressure sensors are generally installed near the ground using long sensing lines so that personnel can easily access the transmitter for replacement or maintenance purposes. However, process connections using sensing lines may be blocked by accumulations of impurities from the fluid. It is important for the sensing lines to be periodically purged, or blown down, in order to remove any foreign fluid and impurities that can degrade the accuracy of pressure transmitters.

Instrument lines can encounter a number of problems that can influence the accuracy and response time of a pressure sensing system. Sensing line problems that have been noticed in NPPs include

- blockages due to sludge, boron, or deposits,
- air or gas entrapped in low-pressure sensing lines,
- frozen sensing lines, and

- leakage from sensing lines.

Any one of these issues can increase the pressure sensing system response time or cause other problems. For instance, blockages, voids, or freezing in sensing lines can cause errors in pressure measurements and also affect the dynamic response of the pressure sensing system. Despite provisions usually made against these problems in the design of sensing lines, experience has shown that they do occur in many NPPs.

In this chapter, signal processing methods for online diagnostics of sensing lines are presented. The development and interpretation of these techniques requires mathematical modelling of the impulse lines, which is accomplished herein using the hydraulic-electric analogy. Results from applying the modelling and diagnostics to instrument lines in operational electric power plants are presented.

2. Background

As mentioned previously, pressure transmitters are sheltered from harsh environmental effects by siting them away from the process. Depending on the application, one or two sensing lines are used to couple a pressure sensor to the process piping, reactor vessel, or primary flow elements. Sensing lines are typically made of small diameter (on the order of 6 mm to 13 mm) stainless steel, carbon steel, or copper tubing in thicknesses of about 2 mm. Tubing is preferred over piping because it can be installed in one piece, reducing the possibility of leaks. Both *liquid-filled* and *gas-filled* impulse lines can be found in NPPs. Liquid impulse lines are typically filled with either the process liquid or oil depending on the sensing line design and application. Gas instrument lines are filled with steam, air, nitrogen, or other gases, and there is sometimes a transition in these lines to another medium, such as oil or water.

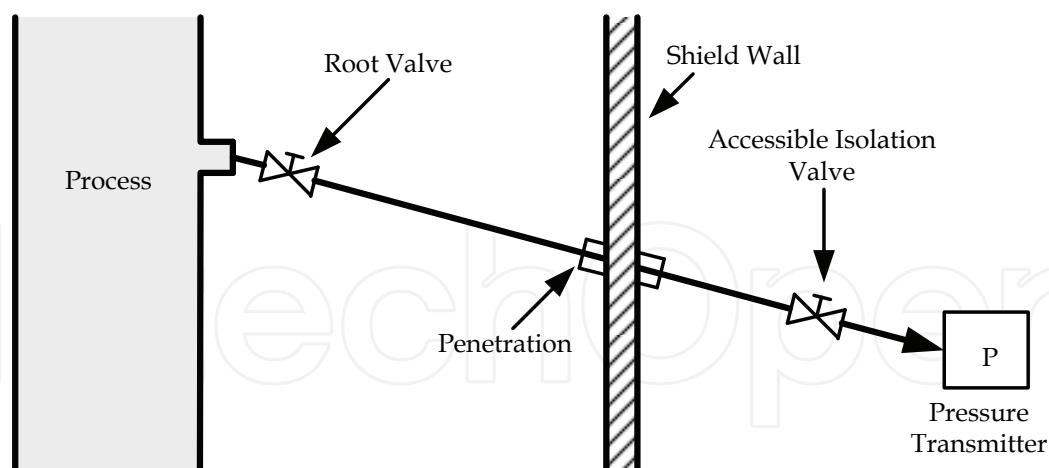


Fig. 1. Typical pressure sensing line inside a nuclear reactor containment.

Sensing lines vary in length, ranging from a few meters to 200 or 300 meters depending on the transmitter location and service in NPPs (Hashemian et al., 1993). Because the overall response time of the pressure sensing system is affected by the instrument line length, impulse lines are made as short as practically possible. Therefore, the average length of sensing lines for safety-related pressure transmitters is usually 10 to 50 meters (Hashemian et al., 1993). Fig. 1 shows a typical pressure sensing line inside a nuclear reactor containment

where the root and isolation valves are employed to connect the sensing line to the process and to a pressure transducer, respectively.

Sensing line installations are designed to allow for thermal expansion and vibration without deformation, to ensure drainage by gravity, and to provide for self-venting. For liquid-filled impulse lines, self-venting is accomplished by slanting the impulse line downward to allow any gas or air in the line to vent to the process. If the instrument line cannot be sloped as required, a high-point vent and low-point drain will be needed for liquid and gas sensing lines, respectively. The mechanical design, engineering, fabrication, installation, testing, and protection of power plant instrumentation sensing and control lines are addressed within industrial standards (ISA, 1999; ISA, 2005; ASME, 2007). These standards establish the applicable installation requirements and limits of instrumentation sensing and control lines and their instruments in both fossil and nuclear power plants.

Blockage, voids, or leaks in sensing lines can cause errors in pressure measurements and can also affect the dynamic response of the pressure sensing system. Although sensing lines are usually designed to avoid these problems, they still occur in industrial processes.

- *Blockage.* Blockages occur in sensing lines when solidification of boron, sludge, and other containments accumulate in the reactor water. Blockages also take place from obstructions because of improper line up or seating of isolation and equalizing valves and crimping of sensing lines. Partial blockages are detrimental only to the dynamic response time of the system and do not normally affect the static output of the system. However, the pressure information is totally lost when the blockage has built up to the level of completely obstructing the line. In addition, sensing line clogs can significantly increase the dynamic response time of pressure systems (Hashemian et al., 1993). Remedies that are practiced in several NPPs to remove deposits from sensing lines are to blow down, back fill, or drain the lines periodically. Condition monitoring based approaches also can be applied to deal with impulse line blockages by detecting their presence.
- *Voids.* Air or gas entrapped in liquid sensing lines can result in false pressure readings, sluggish response, and extraneous noise due to acoustic resonances. For instance, an air pocket in absolute pressure transmitters can cause the pressure indication to be lower than normal in addition to adding a delay in transmission of the pressure information. Voids are difficult to purge from the system, and the problem exists even though high pressures are involved.
- *Leakage.* A sensing line may have a root valve, one or more isolation valves, an equalizing valve, and other connections that can provide opportunities for leakage to happen, especially under high operating pressures. Any significant leakage or loss of fluid from an instrument line can induce a false pressure reading.

Examples of sensing line problems experienced by the U.S. nuclear power industry can be found within the Nuclear Regulatory Commission licensee event report (LER) database. Hashemian et al. (1993) uncovered 551 reports of impulse line problems from approximately 40,000 LERs spanning 1980–1992. Table 1 shows some examples of sensing line problems experienced by the nuclear power industry along with the particular pressure-related variable being sensed. An interesting case of blockage is that of a frozen sensing line. Freezing can take place in fluid sensing lines under cold weather conditions if the heat tracing of the sensing line is aged or damaged, or in the event of power loss. Although the

transmission of pressure ceases when the instrument line is completely frozen, the problem can be overlooked if the static working pressure remains registered by the transducer.

Failure Mode	Specific Problems	Locations of Problems
Blockage	Partial blockage due to sludge build-up Sensing lines plugged with boric acid Obstruction in low pressure line Magnetite in sensing line Frozen sensing line	Steam generator level Boric acid tank level Steam generator flow Steam generator level Steam generator pressure
Voids	Air pocket in low pressure line side Air pocket trapped in sensing line Entrapped air in sensing line	Steam generator level Pressurizer level Reactor water cleanup system flow transmitter
Leakage	Leak in instrument line Leak in upper-seal pressure sensing line due to weld crack from vibration	Safety-related nitrogen level Reactor coolant pump upper-seal cavity pressure

Table 1. Examples of sensing line problems (Hashemian et al., 1993)

The possibility of such pressure sensing line failure modes is an impetus to establish predictive maintenance (PM) programs. Equipment health monitoring is known by a variety of related endeavours including condition-based and reliability-centred maintenance (RCM). Figure 2 illustrates three basic approaches to equipment maintenance. Corrective (or reactive) maintenance is taken only after the component has failed. To avert breakdown, preventive approaches involve anticipatory actions based on a schedule or prediction. Scheduled maintenance, which may involve inspections and/or pre-emptive replacements, can be performed on either calendar or equipment use bases. PM is initiated on the basis of a detected onset of equipment malfunction or failure. RCM incorporates all three approaches while considering the importance of the equipment to the facility mission, and is generally based upon a failure modes and effects analysis.

To accomplish PM without interrupting equipment operation necessitates the use of online monitoring tools for signature analysis. Those signatures, in turn, must be scrutinized to ascertain whether the system or component is trending toward a failure condition. The originating signals are often the result of stochastic (random) processes. The nuclear power industry has traditionally referred to this technique as *noise analysis*. Noise analysis has been used for a variety of nuclear power plant applications including boiling water reactor stability, core barrel motion and moderator temperature coefficient of reactivity determination (Thie, 1981).

The capability to detect faults and to replace the components just prior to failure is desired by industry. By doing so, the consequences of unexpected equipment failures can be avoided. Online component monitoring can yield higher availability, extended life, and reduced costs. Incipient failure detection not only serves to avoid catastrophic failure, but also to assist in planning corrective actions (i.e., preventive maintenance). Incipient failure detection also has the ability to assist in achieving condition-based maintenance objectives. This chapter focuses on developing innovative techniques for detecting blockages, voids, and leakages in the pressure instrument lines.

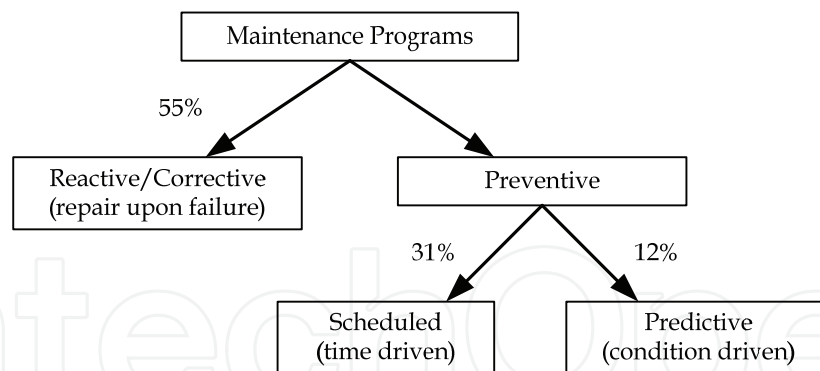


Fig. 2. Equipment maintenance approaches. The percentages represent the categorization of maintenance program in the U.S. from Sullivan et al. (2004) based on a survey in 2000.

3. Sensing Line Modelling

Instrument lines and pressure transmitters are the two major components forming a pressure sensing system. Therefore, to simulate a pressure measuring system, both the sensing line and the pressure transmitter should be modelled. A number of representations have been developed to study pressure transmitters and sensing lines dynamics (Barbero et al., 2000; Bergh & Tijdeman, 1965; Hashemian et al., 1993; Iberall, 1950; Müllens & Thie, 1989). The models presented in this chapter aim at deriving the pressure sensing system transfer function to facilitate the investigation of the pressure signal power spectral densities (PSDs) obtained for noise analysis. These models demonstrate how the system parameters – such as length and cross-sectional area of the sensing line, and the sensing line medium density and sound speed – affect the system transfer function and PSD resonances.

3.1 Hydraulic–Electric Analogy

The hydraulic–electric analogy that relates pressure and flow to voltage and current, respectively, has been well established and applied to a variety of disciplines, including pumping (Gogolyuk et al., 2004), pressure transducers (Clark, 1985), woody plant hydraulics (Tyree & Ewers, 1991), and the human arterial system (Westerhof et al., 1969). The hydraulic (or acoustic) and electrical analogues are summarized in Table 2. Schönfeld (1954) distinguishes between hydraulic and acoustic systems based on the fluid. Specifically, he places incompressible fluids, such as water, into the category of hydraulic systems, whereas acoustical system behaviour is affected by the fluid (*e.g.*, air) elasticity.

General	Electrical	Hydraulic-Acoustic
Flow variable	Current, I	Fluid flow, Q
Potential variable	Voltage, V	Pressure, p
Integrating element	Inductance, L	Inertance, $p = L (dQ/dt)$
Proportional element	Resistance, R	Fluid resistance, $R = p / Q$
Differentiating element	Capacitance, C	Fluid capacitance, $Q = C (dp/dt)$

Table 2. Analogies between electrical and hydraulic systems

The hydraulic–electric analogy also can be employed to the field of pipeline modelling. Consider laminar flow in a tube filled with an incompressible fluid where Q is the fluid

volumetric flow rate. Friction on the tube wall causes a loss of pressure potential, p . The friction-caused potential loss can be expressed as

$$\Delta p = R Q \quad (1)$$

For a round tube in both hydraulic and acoustic systems, the *hydraulic-acoustic resistance* may be represented by (Schönfeld, 1954; Olson, 1957)

$$R = 8 \mu \ell / (\pi r^4) \quad (2)$$

where μ is the dynamic viscosity, ℓ and r are the tube length and radius, respectively. Note that the tube diameter is assumed to be small compared to the tube length so that the end correction may be neglected. Expressions for R must be developed based upon the unique flow characteristics of a given system.

Consider a variable flow rate through a tube for both hydraulic and acoustic systems. Ignoring friction for the moment, a potential difference is required to accelerate or to decelerate the flow, amounting to

$$\Delta p = L dQ/dt \quad (3)$$

The factor L is called the *hydraulic-acoustic inertance* of the system and can be written as (Schönfeld, 1954)

$$L = \rho \ell / A \quad (4)$$

where A is the tube cross-sectional area and ρ is the fluid density. Similar to R , system-specific L expressions must be derived for diverse hydraulic-acoustic systems.

Hydraulic-acoustic potential energy is associated with the compression of a fluid or gas. Hydraulic-acoustic energy increases (decreases) as the fluid is compressed (expanded). *Hydraulic-acoustic capacitance* is the element that opposes a change in the applied pressure. The pressure in terms of the volume displacement, ΔV , can be expressed as (Olson, 1957)

$$p = c^2 \rho \Delta V / V \quad (5)$$

where V is the initial volume and c is the acoustic velocity of fluid in the sensing line. The hydraulic-acoustic capacitance, C , is defined via

$$p = \Delta V / C \quad (6)$$

From Eqs. (5) and (6), the acoustic capacitance of volume V is

$$C = V / (\rho c^2) \quad (7)$$

Physically speaking, the hydraulic-acoustic capacitance is used to represent a cavity or small volume with rigid boundaries.

For example, Hashemian et al. (1993) represented a pressure sensing system by a spring mass system as shown in Fig. 3. As the process pressure changes, the pressure surge is transmitted through the sensing line resulting in a volume change (ΔV_t) in the transmitter cavity. To describe the relationship between the volume change in the transmitter and the pressure required to induce the volume change, a term called *transmitter compliance* is employed. For a pressure change of Δp_s , the transmitter compliance (C_t) can be expressed using Eq. (6) as

$$C_t = \Delta V_t / \Delta p_s \quad (8)$$

Typical units for the compliance are cm^3/bar .

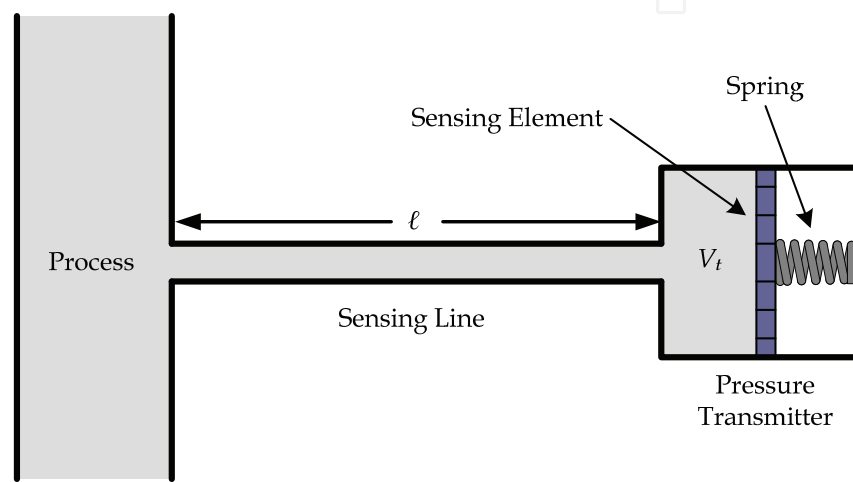


Fig. 3. Spring mass model of a pressure sensing system; after Hashemian et al. (1993).

3.2 Lumped Parameter Model Using Hydraulic-Electric Analogy

By applying the hydraulic–electric analogy, pressurized lines can be represented using electrical circuits, that is, a hydraulic tube is realized as an electric power transmission line. Therefore, similar to transmission line modelling, there are multiple circuit topologies (see Fig. 4) that can be used to accomplish sensing line lumped parameter modelling. The circuit parameters in Fig. 4 can be expressed as

$$R = \frac{8\mu\ell}{\pi r^4}; \quad L = \frac{\rho\ell}{\pi r^2}; \quad C = \frac{\pi r^2\ell}{\rho c^2} \quad (9)$$

Using the simple electrical circuit model of a hydraulic tube, as shown in Fig. 4(a), the transfer function between the input p_i and output p_o pressures can be derived as

$$\frac{p_o}{p_i} = \mathbf{H}_s(j\omega) = \frac{1/(j\omega C)}{R + j\omega L + 1/(j\omega C)} \quad (10)$$

This L -shaped model is a classic underdamped second-order system with a resonant frequency of

$$\omega_{s0} = \frac{1}{\sqrt{LC}} = \frac{1}{\ell/c} \quad (11)$$

The *pi*- and *tee*-shaped representations shown in Figs. 4(b) and 4(c), respectively, are referred to here as the general cases which share an identical transfer function of

$$\mathbf{H}_G(j\omega) = \frac{1}{(1 - \omega^2 LC/2) + j\omega RC/2} \quad (12)$$

which has a resonant frequency of

$$\omega_{G0} = \sqrt{\frac{2}{LC}} = \frac{\sqrt{2}}{\ell/c} \quad (13)$$

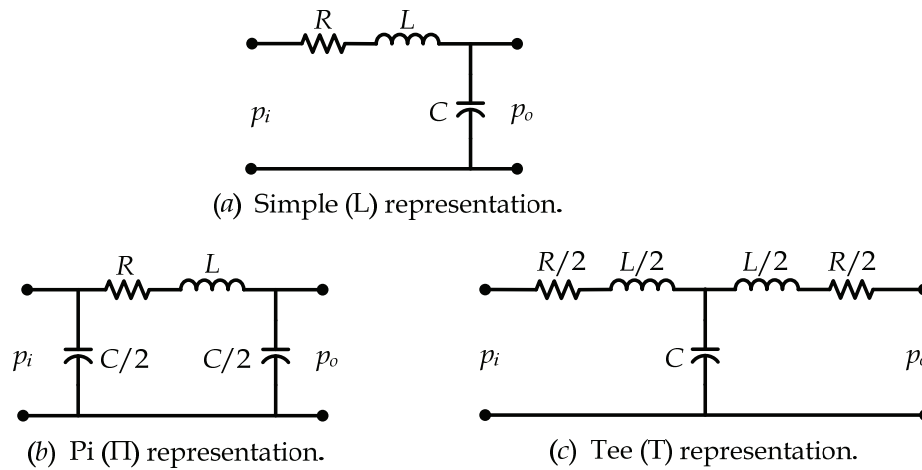


Fig. 4. Sensing line lumped parameter circuit models.

3.3 Sensing Line Model with Linear Distributed Parameters

The analytical solution for unsteady flow problems is obtained by using equations for continuity, momentum, and energy. These equations correspond to the physical principles of mass conservation and energy conservation. Applying these equations leads to a coupled nonlinear set of partial differential equations. After linearization, two linearized partial differential equations describing flow continuity and momentum can be derived as (Matko et al., 2000; Matko & Geiger, 2002; Izquierdo & Iglesias, 2002; Izquierdo et al., 2004):

$$L \frac{\partial Q}{\partial t} + R' Q = -\ell \frac{\partial p}{\partial x} \quad (14)$$

$$C \frac{\partial p}{\partial t} = -\ell \frac{\partial Q}{\partial x} \quad (15)$$

where x is distance along a pipe, t is time, and $R' = (\ell \rho f \bar{Q}) / (A^2 2r) = 2R$ with f being the dimensionless Darcy-Weisbach friction factor ($f = 64/\text{Re}$ for laminar flow), and \bar{Q} being the

average fluid volumetric flow rate. Solving Eqs. (14) and (15) by using initial fluid conditions, the linearized pressurized line model can be written as:

$$Q_i = \frac{1}{Z_c} \sinh(\sqrt{(R'+sL)sC}) p_o + \cosh(\sqrt{(R'+sL)sC}) Q_o \quad (16)$$

$$p_i = \cosh(\sqrt{(R'+sL)sC}) p_o + Z_c \sinh(\sqrt{(R'+sL)sC}) Q_o \quad (17)$$

where $Z_c = \sqrt{(R'+sL)/(sC)}$ is called the *characteristic impedance*, and Q_i and Q_o are the input and output flow rates, respectively. Therefore from Eq. (17), the “exact” transfer function for pipe pressure can be expressed as (Matko et al., 2000):

$$\mathbf{H}_E(s) = \frac{p_o}{p_i} = \frac{1}{\cosh(\sqrt{(R'+sL)sC})} \quad (18)$$

The approximate resonant frequencies of the exact model can be derived as (Lin & Holbert, 2009a):

$$\omega_{En} = \frac{n\pi}{2\sqrt{LC}}, \quad n = 1, 3, 5, \dots \quad (19)$$

The exact formula of Eq. (18) can be approximated by a second-order system (Matko et al., 2000):

$$\mathbf{H}_A(s) = \frac{1}{[LC/2 + (R'C)^2/24]s^2 + R'Cs/2 + 1} \quad (20)$$

which has a resonant frequency at $\omega_0 \approx \sqrt{2/(LC)}$ — the same as the pi and tee models given in Eq. (13).

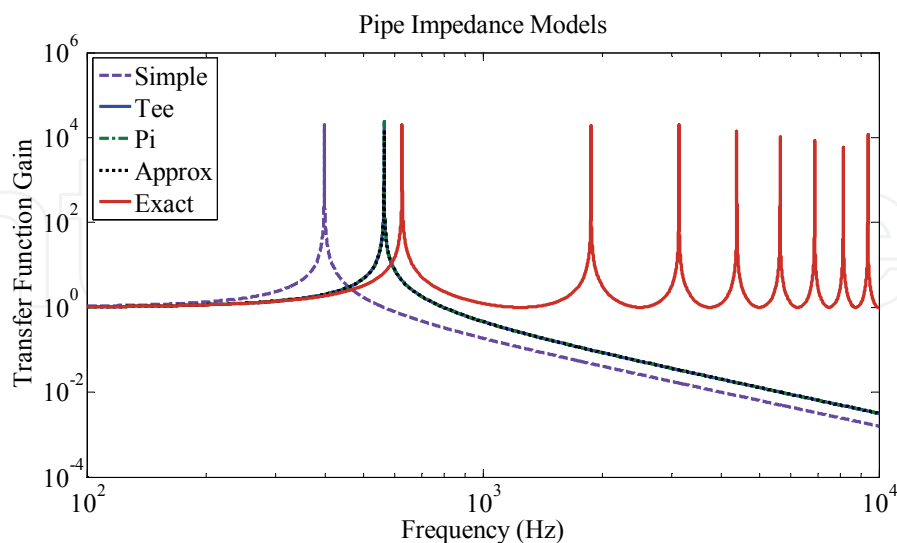


Fig. 5. Transfer functions for the exact (\mathbf{H}_E), pi and tee (\mathbf{H}_C), simple L (\mathbf{H}_S), and approximate (\mathbf{H}_A) pipeline models. The pi, tee and approximate models overlay one another. The pipe system parameters are $\ell = 60$ cm; $r = 0.8$ cm; $\mu = 0.01$ g/cm s; $\rho = 1$ g/cm³; $c = 150,000$ cm/s; $Re = 1000$; and $\bar{Q} = 6.25$ cm/s.

Lin and Holbert (2009a) compared the hydraulic–electric models described previously as shown in Fig. 5. The pi and tee models are nearly identical to the approximation of the exact model. Therefore, the pi and tee models are considered more accurate than the simple (L) expression. However, it can be recognized in Fig. 5 that the resonant frequencies of the pi, tee and approximate models do not match the fundamental resonant frequency of the exact model. Besides, the pi, tee and approximate models only reveal the first resonant peak and its location in the frequency domain while the exact model exhibits multiple resonant peaks. Furthermore, a high frequency roll-off appears in non-exact cases.

3.4 Equivalent Pi Circuit

In order to facilitate the implementation of the pipeline exact model for complex pressure system modelling, an equivalent circuit is introduced. The circuit shown in Fig. 6 is called an *equivalent pi circuit* that has been used in power transmission line modelling (Glover & Sarma, 2000). From Fig. 6, p_i and Q_i can be expressed in terms of p_o and Q_o as

$$p_i = \left(1 + \frac{Z}{Y}\right)p_o + ZQ_o \quad (21)$$

$$Q_i = \frac{1}{Y}\left(2 + \frac{Z}{Y}\right)p_o + \left(1 + \frac{Z}{Y}\right)Q_o \quad (22)$$

By comparing the coefficients of Eqs. (17) and (21), Z and Y are recognized as:

$$Z = Z_c \sinh\left(\sqrt{(R' + sL)sC}\right) \quad (23)$$

$$Y = \frac{Z_c \sinh\left(\sqrt{(R' + sL)sC}\right)}{\cosh\left(\sqrt{(R' + sL)sC}\right) - 1} \quad (24)$$

Overlays (not shown) of the transfer functions from the exact model and the equivalent pi representation are identical, as expected since the theory in Glover and Sarma (2000) shows them to be equal. In other words, the equivalent pi circuit representation yields the same frequency response as the exact model, *i.e.*, $\mathbf{H}_Z = \mathbf{Y}/(\mathbf{Y} + \mathbf{Z}) = \mathbf{H}_E$; there is no approximation involved.

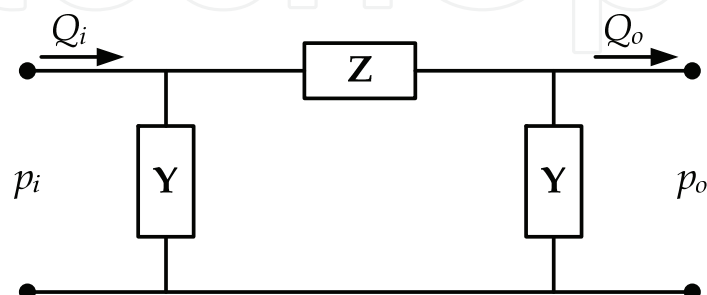
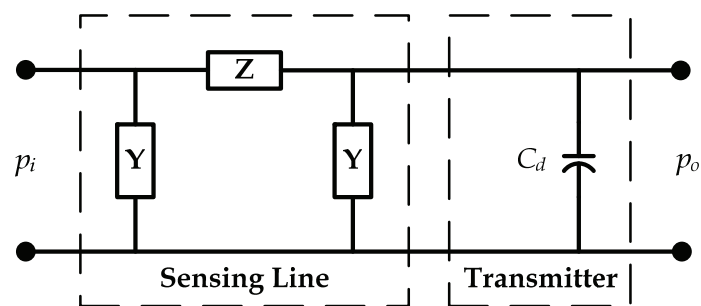


Fig. 6. Equivalent pi circuit for pressure sensing line exact model.

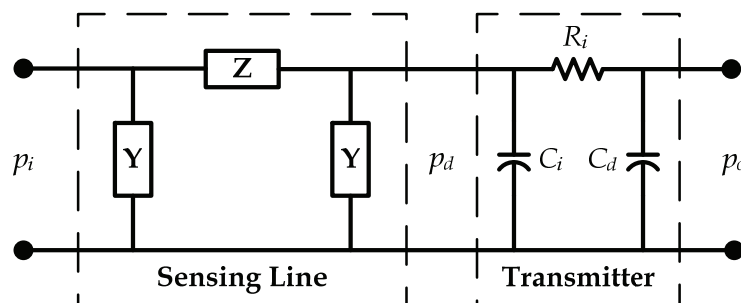
4. Sensing Line Diagnostics

In the previous section, various sensing line models have been presented, and the sensing line equivalent pi circuit representation is considered more accurate and easier to implement for impulse line diagnostics. To cooperate with the equivalent pi model of sensing lines, pressure sensor lumped parameter models are introduced here.

Typically, two types of pressure transmitters—motion-balance and force-balance—are used for safety-related pressure measurement in nuclear power plants. The major difference between them is how the movement of the sensing element is converted into an electrical signal. The transmitter modelling focuses on the component before the pressure-to-electrical signal conversion step. Therefore, the sensor representation presented here is valid for both types of pressure transducers.



(a) Pressure sensing system model with single diaphragm sensor representation



(b) Pressure sensing system model with inner structure sensor representation

Fig. 7. Two pressure sensing system models.

The simplest expression for a pressure transmitter is a single diaphragm. The diaphragm capacitance can be defined as

$$C_d = \Delta V_d / p_o \quad (25)$$

where ΔV_d is the displaced diaphragm volume and p_o is the pressure at the diaphragm at instant t . Hence, the pressure system model can be represented as shown in Fig. 7(a). However, this simple model may not be adequate in some cases. For example, the simple representation has been proved insufficient for understanding the laboratory measurements performed with a Rosemount capacitive transmitter (Blázquez & Ballestín, 1995). The reason is that the Rosemount sensors have an inner structure for pressure reduction. A low frequency real pole resulting from the inner structure dominates the frequency response of

the sensor. Therefore, the model should be modified as shown in Fig. 7(b). The inner structure of the Rosemount transmitter can be modelled with (Barbero et al., 2000):

- an isolating diaphragm (membrane) with capacity C_i ,
- a filling fluid of silicone oil instead of water,
- a smaller channel cross-section than that of the sensing line,
- a large resistance R_i for pressure reduction compared to sensing line ($R_i \gg R$), and
- a sensing diaphragm C_d .

4.1 Sensing Line Blockage

Extending the pressure sensing system model to a situation of blockage, one comes to the realization that all three parameters (R , L , and C) change (see Eq. (9)) as the original tube inner radius (r_i) decreases. The flow area reduction, as shown in Fig. 8, is denoted as $b = (r_B/r_i)^2$ where r_B is the pipe radius due to blockage.

The transfer function of a pressure sensing system consisting of a 50-meter long water-filled impulse line and an inner structure pressure transmitter was numerically computed for several cases: normal conditions and varying degrees of blockage. The effect of blockage on the transfer function is initially studied as shown in Fig. 9. From Fig. 9, it can be observed that the first resonant peak moves toward a lower frequency and the rest of the resonant peaks shift slightly toward lower frequencies as the blockage amount increases. In addition, all the resonant peak magnitudes are reduced as the blockage becomes larger. The effects on the transfer function under high blockage circumstances are demonstrated in Fig. 10. The impacts of severe blockages are consistent with what occurs in the earlier blockage cases (Fig. 9).

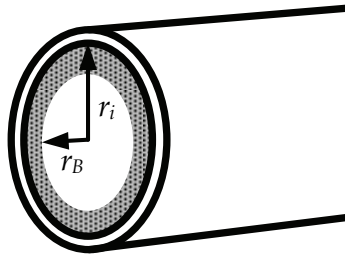


Fig. 8. A pipe with a uniform blockage amount along its length.

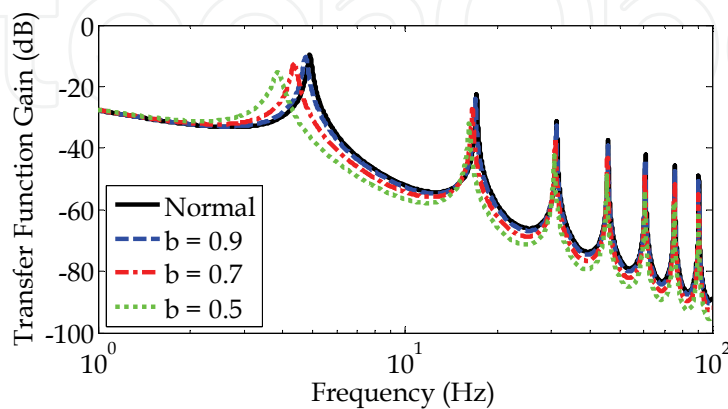


Fig. 9. Transfer functions of a pressure sensing system under normal condition and with sensing line blockages.

However, the first resonant peak disappears when the blockage reaches a certain level and the adjacent resonant peaks vanish one by one as the blockage level keeps increasing. Note the first four peaks of the transfer function with 0.01 cross section ratio (b) have disappeared in Fig. 10 while the remaining peaks are obscure but still exist. Moreover, the transfer function gain is considerably reduced with severe blockage occurring.

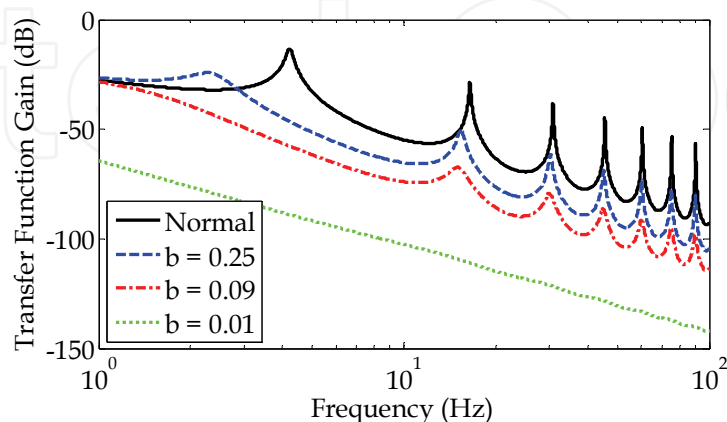


Fig. 10. Transfer functions of a pressure sensing system under normal condition and with severe blockages.

4.2 Sensing Line Voids

When voids (bubbles) appear inside a liquid-filled sensing line, the sensing line now contains a two-phase fluid. Bubbles can blend into the instrument line medium either homogeneously or heterogeneously. These two different mixing situations influence the transmitted signal differently. In this subsection, the sensing line fluid and the void media used for the studies are water and air, respectively. Another possible two-phase fluid is simply a water liquid-vapour mixture.

A homogeneous air-water mixture exists only when the air volume fraction is less than one percent (Sherstyuk, 2000). In the presence of air bubbles, the total volume inside the sensing line is the sum of the air volume, V_a , and water liquid volume, V_w , and the density of the air-water mixture can be expressed as (Barbero et al., 2000)

$$\rho_m = \beta \rho_a + (1 - \beta) \rho_w \quad (26)$$

where ρ_a and ρ_w are the air and water densities, respectively, at normal system pressure, and β is the void fraction by volume, $\beta = V_a / (V_a + V_w)$. The dynamic viscosity of a two-phase fluid can be estimated using the Grunberg equation (Grunberg & Nissan, 1949):

$$\ln \mu_m = X \ln \mu_a + (1 - X) \ln \mu_w + X(1 - X)d \quad (27)$$

where μ_a and μ_w are the air and water dynamic viscosities, respectively, at normal pressure, X is the void mole fraction, and d is the interaction parameter. The interaction parameter can be set to zero for the mixture of similar non-polar components so that the last term of Eq. (27) can be neglected. Consequently, Eq. (27) can be reduced as:

$$\ln \mu_m = X \ln \mu_a + (1 - X) \ln \mu_w. \quad (28)$$

By replacing the mole fraction with other parameters, Eq. (28) can be modified as:

$$\ln \mu_m = \frac{\beta \rho_a A_w}{(1 - \beta) \rho_w A_a + \beta \rho_a A_w} \ln \mu_a + \frac{(1 - \beta) \rho_w A_a}{(1 - \beta) \rho_w A_a + \beta \rho_a A_w} \ln \mu_w \quad (29)$$

where A_w and A_a are molar masses for water and air, respectively.

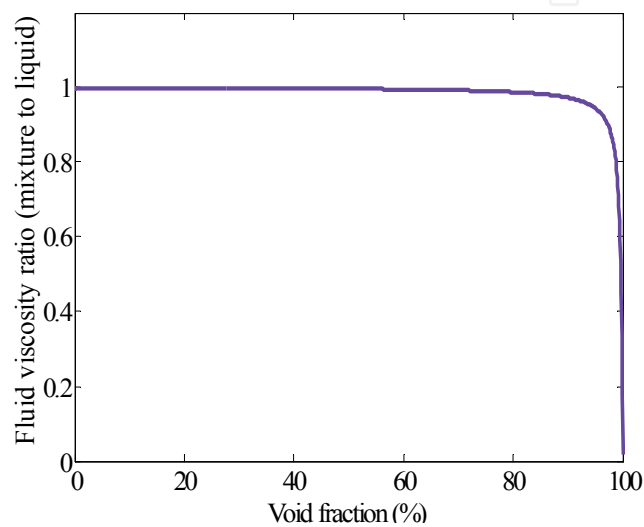


Fig. 11. The variation of the viscosity within a water-air mixture.

The variation of the viscosity within a water-air mixture is shown in Fig. 11. The density and dynamic viscosity changes affect the impulse line inductance (L) and resistance (R), respectively. However, the sensing line capacitance (C) varies much more than R and L not only through ρ but also via the sound velocity. Therefore, the sound velocity variation within a two-phase fluid is discussed below. Note that the voids are most likely air or water vapour; and the sensing line void model developed herein is valid for both cases.

A two-phase fluid has the elasticity of a gas and the density of a liquid (Barbero et al., 2000) so that the sound velocity decreases significantly, and consequently C increases. For a homogeneous mixture, the sound velocity can be calculated as (Landau & Lifshitz, 1959)

$$\frac{1}{c^2} \equiv \frac{\partial \rho}{\partial p} \quad (30)$$

Substituting with Eq. (26), Eq. (30) can be written as (Barbero et al., 2000)

$$\frac{1}{c^2} \equiv \frac{\partial \rho_w}{\partial p} (1 - \beta) + \frac{\partial \rho_a}{\partial p} \beta + (\rho_a - \rho_w) \frac{\partial \beta}{\partial p} \quad (31)$$

Mass conservation in the impulse line is applied to calculate the change in void fraction with pressure. With m_a and m_w corresponding to the air and liquid water masses, respectively,

$$\frac{m_a}{m_w} = \frac{\rho_a \beta}{\rho_w (1 - \beta)} \quad (32)$$

Taking the partial derivative with respect to pressure at both sides of Eq. (32) and noting that m_a/m_w is a constant, the partial derivative of the void fraction with respect to pressure can be derived as

$$\frac{\partial \beta}{\partial p} = \beta(1 - \beta) \left(\frac{1}{\rho_w c_w^2} - \frac{1}{\rho_a c_a^2} \right) \quad (33)$$

Substituting Eqs. (30) and (32) into Eq. (31), the sound velocity within a homogeneously mixed fluid, after some algebraic manipulations, is found to be

$$\frac{1}{c_{hom}^2} = \frac{1 - \beta}{c_w^2} + \frac{\beta}{c_a^2} + \beta(1 - \beta)(\rho_a - \rho_w) \left(\frac{1}{\rho_w c_w^2} - \frac{1}{\rho_a c_a^2} \right) \quad (34)$$

where c_a and c_w are the sound velocities in the air and water phases, respectively.

Fig. 12 shows the theoretical sound velocity variation within a homogeneous water-air mixture that has been experimentally proved (Gibson, 1970; Kafesaki et al., 2000); however, a homogeneous mixture has only been considered applicable when the air fraction (β) is less than 1% (Sherstyuk, 2000).

The transfer function of a pressure system with voids in the sensing line under the homogeneous mixture condition is shown in Fig. 13. The simulation is based on a pressure sensing system consisting of a 10-meter long water-filled impulse line and a single diaphragm pressure transmitter. As mentioned before, the homogeneous case is valid under the condition that the gas fraction is less than 1% (Sherstyuk, 2000). Hence, Fig. 13 shows the transfer functions for small amounts (< 1%) of air occurring within the impulse line. For the homogeneous mixture case, the appearance of bubbles makes significant feature changes to the original system transfer function curve as shown in Fig. 13. It can be seen that all resonant peaks shift dramatically toward lower frequencies. However, in a sensing line absent of flow, gas and liquid components eventually separate into a heterogeneous arrangement, which is now addressed.

Similar to the homogeneous air-water mixture case, a method that replaces the original R , L , and C parameters with new values calculated using the modified fluid density and sound velocity can be applied to the heterogeneous air-water mixture case (Barbero et al., 2000) as depicted in Fig. 14(a). By using this method, the network topology of the pressure sensing line model remains unchanged based on the void location, although the model parameters are affected. However, based on test results from the Kingston steam plant (Schohl, 1987a; Schohl, 1987b; Schohl et al., 1987; Schohl & Vigander, 1989), different air locations cause distinct effects on the pressure noise spectrum. Specifically, air present near the midpoint of the sensing line affects resonant frequencies much more than does air close to the beginning of the line.

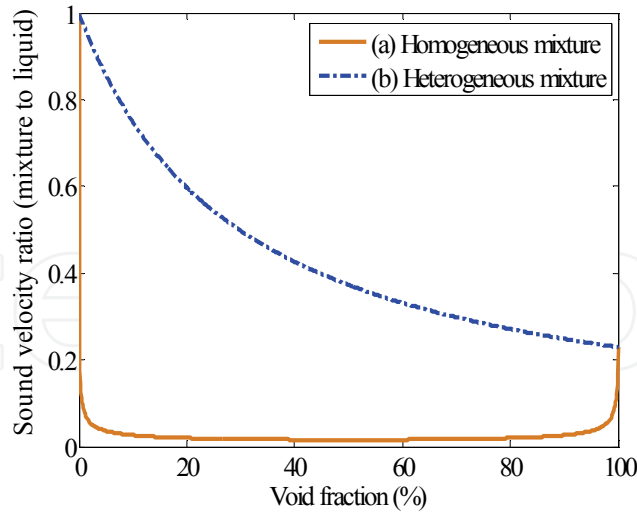


Fig. 12. Sound velocity variation within water–air mixtures.

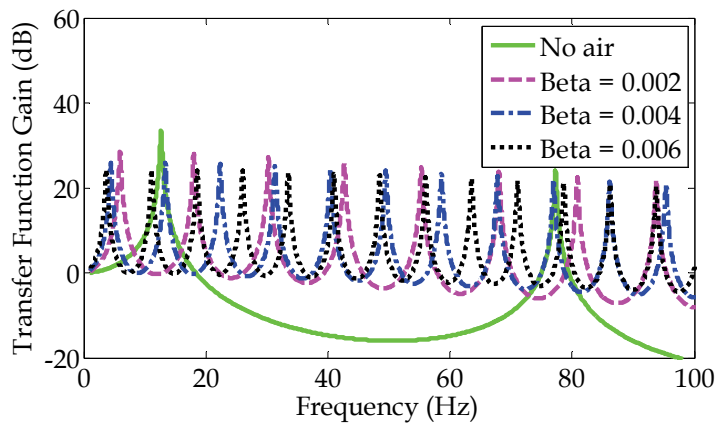


Fig. 13. Transfer functions of a pressure sensing system with air voids homogeneously mixed with the water fluid in the impulse line. Beta is the volumetric void fraction (β). The pipe system parameters are $\ell = 10$ m; $r = 6$ mm, $\mu = 0.004$ kg/m s; $c = 1500$ m/s; $\rho = 1000$ kg/m³; $Re = 1000$; and $\bar{Q} = 37.7$ cm³/s.

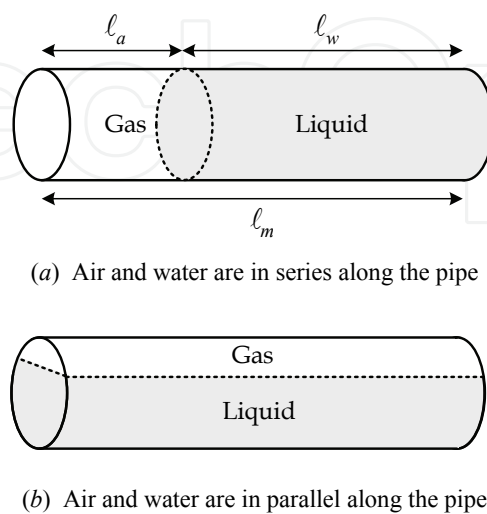


Fig. 14. Heterogeneous gas–liquid mixture geometries.

Another way to simulate the heterogeneous air-water mixture is to model an air section of length ℓ_a within a tube by an acoustic capacitor that is calculated using a lumped parameter representation (Müllens and Thie, 1985)

$$C_a = (\pi r^2 \ell_a) / (\rho_a c_a^2). \tag{35}$$

By using this depiction, sensing lines with voids occurring at different locations can be represented by the sensing line models as exemplified in Fig. 15. Note that the lumped parameter representation of voids is not applicable for the heterogeneous air-water mixture shown in Fig. 14(b), where the arrangement of air and water layers is in parallel along the pipe.

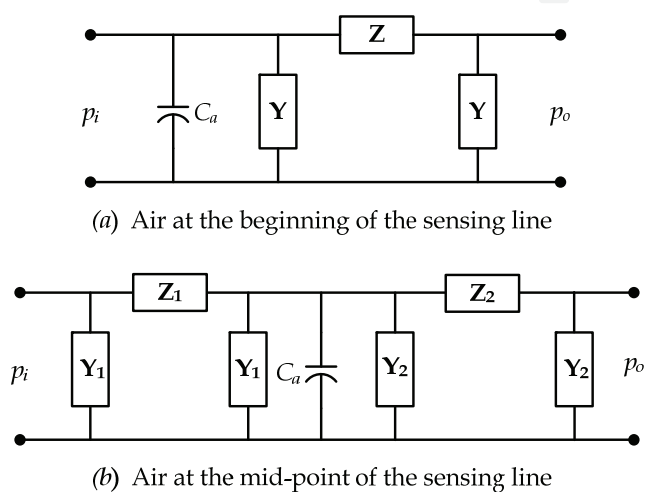


Fig. 15. Circuit models of tubes with voids occurring at different locations.

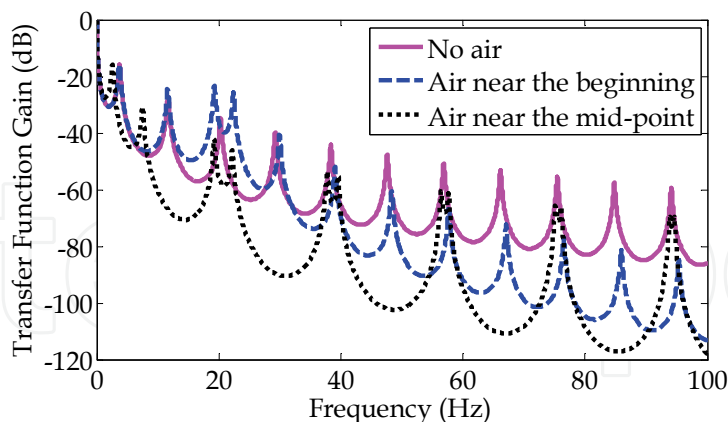


Fig. 16. Transfer functions of a water pressure system with air voids at the beginning and mid-point of the sensing line. The volumetric void fraction (β) is 0.0001.

Fig. 16 shows the transfer functions based on the lumped parameter void model for identical air pockets placed at two different locations along the sensing line. In the first case, an air pocket is positioned close to the beginning of the tube, and in the second instance, the air is located near the mid-point of the impulse line. It can be observed from Fig. 16 that even though the air volumes for both pockets are equal, the system transfer functions vary

significantly depending on where the void is located. These differences in transfer functions are physically attributable to the nonlinear system behaviour that results from site-dependent sound speed differences due to the air position (Barbero et al., 2000) as well as the concomitant changes in the standing wave frequencies (Schohl & Vigander, 1989).

4.3 Sensing Line Leakage

Leakage from a sensing line may be represented using the orifice equation of

$$Q = C_f A \sqrt{2\Delta p / \rho} \quad (43)$$

where C_f is a flow coefficient, and A is the flow area of the leak. The linearized orifice equation is

$$\delta p = \frac{\rho Q_0}{(C_f A)^2} \delta Q \quad (44)$$

where Q_0 is the steady-state leakage flow rate. The leak therefore becomes a parallel resistive term in the sensing line model. The equivalent resistance obtained from the linearized version of the orifice equation relating steady-state flow, Q_0 , and pressure, p_0 , provides two functional forms, specifically, $R = \rho Q_0 / (C_f A)^2 = \sqrt{2\rho p_0} / (C_f A)$. Generally, the flow coefficient, C_f , ranges from 0.6 for sharp edges to 1.0 for rounded edges. The former expression for R is more useful for determining the leakage amount (Q_0) from a PSD, whereas the latter expression is appropriate for selecting R values to perform initial scoping analyses based on the primary coolant system pressure (p_0). Using the equivalent pi representation, the leak may be placed at an arbitrary position along the sensing line, as depicted in Fig. 17.

Using the model of Fig. 17, a 50-m long, 2-cm diameter sensing line was simulated with a 1-mm diameter leak. The leak position was varied, specifically, at 25%, 50% and 80% of the tube length. The transfer function results shown in Fig. 18 demonstrate that although the resonant peak frequencies do not change, the peak amplitude does. In particular, the magnitude of the peak at the fundamental frequency decreases as the leak position moves from the inlet to the outlet, but other harmonics do not necessarily exhibit the same pattern. Such results are consistent with the theoretical and experimental observations by Lee et al. (2005; 2006) who found that the pattern of peak magnitude change can be utilized to determine the position of a leak in a pipeline. For large leaks, the fundamental resonant peak location also shifts to higher frequencies, as shown in Fig. 19.

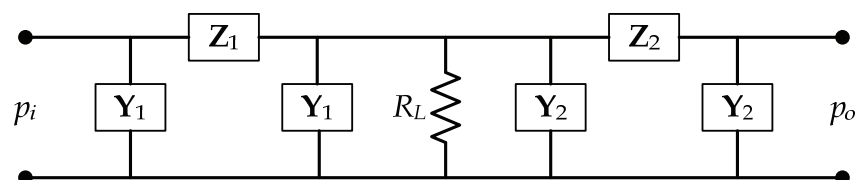


Fig. 17. Sensing line with leak somewhere between the sensing line inlet and outlet.

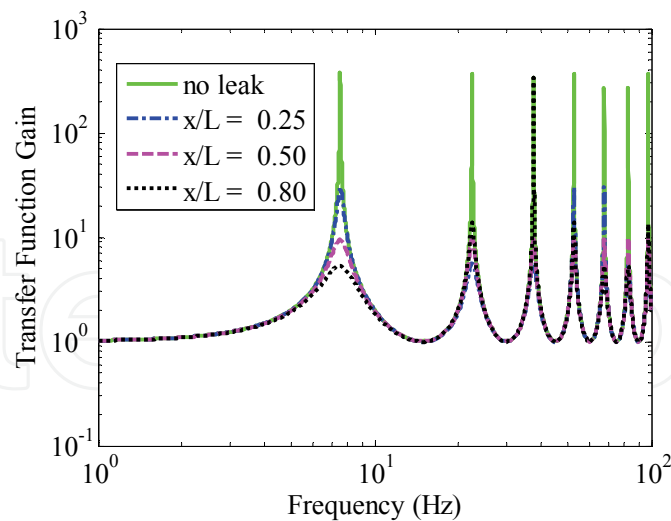


Fig. 18. Effect on sensing line transfer function by the position (x) of a 1-mm diam. leak within a 50-m long (L), 2-cm diam. sensing line with water at 15 MPa and 300°C.

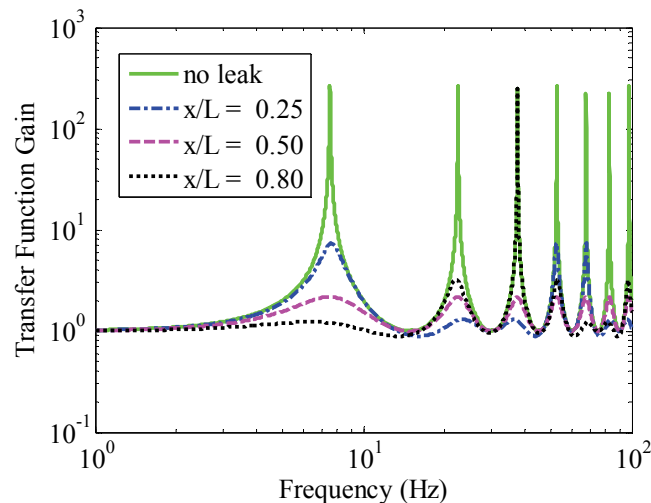


Fig. 19. Effect on sensing line transfer function by the position (x) of a 2.5-mm diam. leak within a 50-m long (L), 2-cm diam. sensing line with water at 15 MPa and 300°C.

5. Operational Data Analysis

In the previous section, the modelling of sensing line anomalies using the equivalent pi circuit representation has been presented. Operational data from a pressurized water reactor (PWR) and a coal-fired power plant are analyzed in this section to compare to the sensing line fault modelling.

5.1 Sensing Line Blockage in a PWR

Steam pressure measurements were taken from four steam generators. The four steam generators are identical so that the four pressure sensing systems are deemed similar to one another. Twenty minutes of pressure noise data were acquired using a 200 Hz sampling frequency with a low-pass filter cut-off of 67 Hz. Two different data sets were obtained

approximately three years apart under (1) normal (unblocked) conditions and (2) when the pressure sensing line of one transducer was blocked.

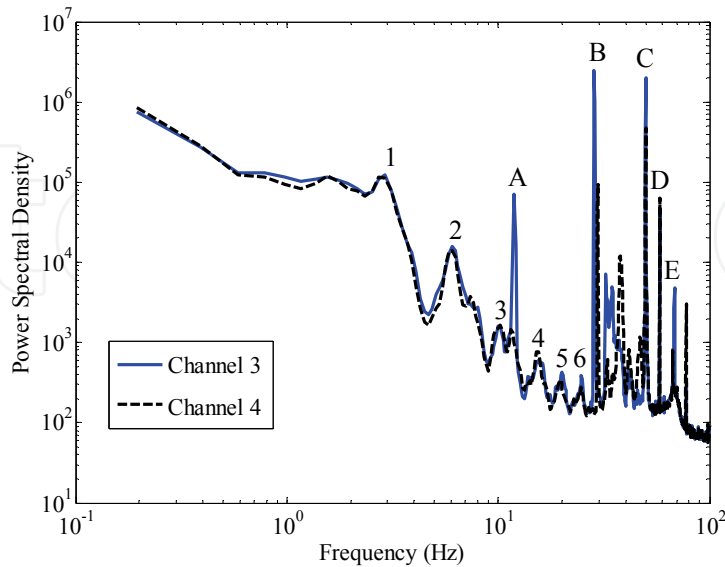


Fig. 20. PSDs of normal steam pressure noise data acquired at 200 Hz sampling frequency from Channels 3 and 4 (Lin & Holbert, 2009b).

Fig. 20 shows the PSDs of the noise signals obtained from Channels 3 and 4 before blockage occurs. There are a number of peaks in Fig. 20 for each PSD; however, some of the peaks originate from the other noise sources. Therefore, it is essential to identify the resonant peaks associated with the pressure sensing system. From Eq. (19) and simulation results for complete pressure sensing systems, it is known that the peak intervals are roughly equivalent. Based on this pattern, the resonant peaks caused by the pressure sensing system are enumerated as indicated in Fig. 20. To verify the peak recognition, the PSD from Channel 3 is compared to that from Channel 4. It can be seen in Fig. 20 that the two PSDs are almost identical up to the sixth peak while the higher frequency portion of the PSDs is not as similar as it is in the lower frequency region. The higher frequency data are corrupted by other noise sources. For example, peak C in Fig. 20 is the 50 Hz electrical noise. Because the data from both channels were measured through two similar pressure sensing systems, the shared resonant peaks are considered related to the pressure sensing system which agrees with the peak recognition result based on the uniform peak interval.

Fig. 21 shows the PSDs of the noise signals acquired from the blocked (Channel 3) and the normal (Channel 4) pressure sensing systems, respectively. It can be seen in Fig. 21 that the first three resonant peaks of Channel 3 have vanished due to the blockage and the magnitudes of the fourth and the sixth peaks are reduced significantly which is consistent with the severe blockage simulation result shown in Fig. 10. However, the PSD curve near the fifth peak location rises abnormally which is not found from the simulation result. This could be the result of plant equipment or operational variation since the normal data and abnormal data were taken three years apart. It is possible that the 1% upgrade in power for the NPP in the interim affected the later data.

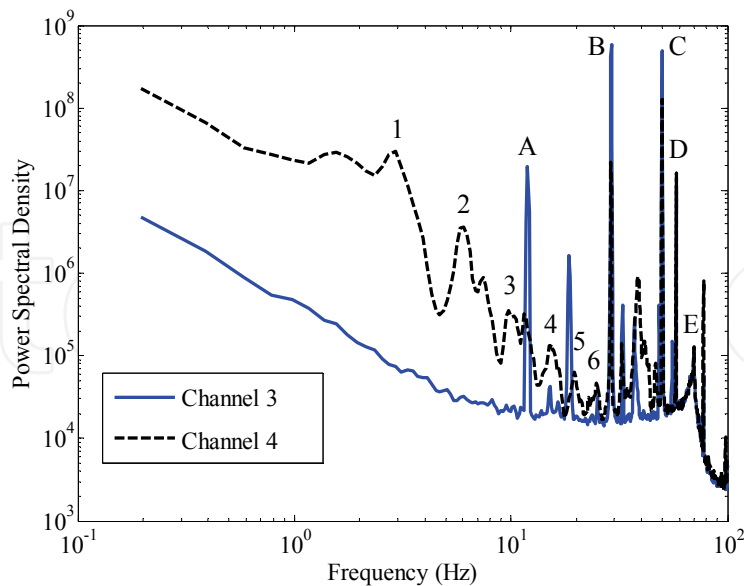


Fig. 21. PSDs of blocked and normal steam pressure noise data acquired at 200 Hz sampling frequency from Channels 3 and 4, respectively (Lin & Holbert, 2009b).

Based on Parseval's Theorem, the integral of the PSD is directly proportional to the signal variance (σ^2). From Figs. 9 and 10, it can be observed that the area under the transfer function curve of the pressure sensing system decreases as blockage increases. Therefore, in general, a reduced root mean square (rms), σ , noise level is anticipated for a blocked sensing line. However, this is not the case for the operational data presented here because, as mentioned above, the data are corrupted by other noise sources that manifest themselves in the higher frequency range of the PSDs shown in Figs. 20 and 21. In particular, there are several high frequency components appearing in the Channel 3 (blocked) PSD and with greater peak magnitudes as compared to the Channel 4 (normal) PSD. For this particular case, an alternative analysis method could be based on integrating the PSD up to and slightly past the sixth peak (i.e., before peak B).

5.2 Sensing Line Voids in a Fossil Unit

Field tests for void detection were conducted at the Kingston steam plant (Schohl, 1987a; Schohl, 1987b; Schohl et al., 1987; Schohl and Vigander, 1989) where nine coal-fired generating units are operating. A depiction of the sensing line for pressure measurement at the discharge of the Unit 1 raw water service pump is shown in Fig. 22. The 1.02-cm diam. copper line has a total length of approximately 80.5 m including an elevation gain of about 13.7 m from the pump, located in the power plant basement, to the control room pressure gauge. There are three tees along the line. Two of them were installed near the pump and the condenser respectively to provide locations for air injection. The third tee was placed under the control room (807) for attachment of a hydrophone.

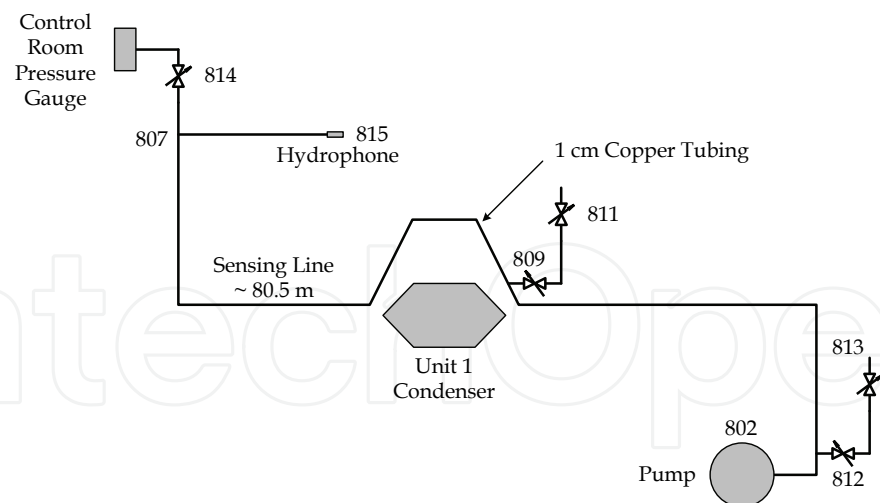


Fig. 22. Schematic of Kingston Unit 1 raw water service pump pressure impulse line, adapted from (Schohl, 1987a).

For the tests, the effects of the control room pressure gauge were removed by closing the in-line isolation valve (814) below the gauge. Then, measurements (termed “pseudo no-air” for reasons which will be explained later) taken after attempting to purge the line of air were compared with measurements recorded after air was inserted either close to the pump or near the condenser. The background flow noise was measured using the hydrophone at 815. To remove the random signal content, leaving the periodic components, spectra obtained from 40 consecutive time records, each 8 seconds long, were averaged together (Schohl, 1987a). Fig. 23 shows the effects of air added into the sensing line on power spectra of the flow noise with respect to air near the pump. According to Schohl (1987a), electrical noise appears in the PSD at 60 Hz, and pump first and second order harmonics occur at 29 Hz and 58 Hz, respectively. From Fig. 23, it can be recognized that added air manifests itself as an additional peak at 24.2 Hz, as noted by Schohl (1987a). This peak corresponds to surge oscillation of the column between the process line and the inserted air. Besides, except for the peak near 44 Hz, the resonant frequencies greater than 24 Hz are all moved slightly toward higher frequencies because of the added air.

In order to verify the developed pressure sensing system model, the raw water sensing line system (see Fig. 22) is represented using a five-segment impulse line equivalent pi circuit, as shown in Fig. 24, with the hydrophone and air realized by a single diaphragm capacitor, $C_d = \Delta V_d / p_o$, and acoustic capacitors, via Eq. (35), respectively. According to the Kingston test report (Schohl, 1987a), this sensing line was not equipped with air bleed lines so that there was no way to confidently purge all air from the line. Furthermore, the trapped air in the sensing line was distributed among several locations, with each location holding a small air pocket, rather than centralized at one location as a single large void. Therefore, in the network of Fig. 24, two small air pockets realized by two acoustic capacitors are inserted, respectively, at locations 809 and 814 which are two higher positions (see Fig. 22) considered more likely to trap air. Hence, we refer to these results as the “pseudo no-air” cases because of the two trapped air pockets which are included in the model.

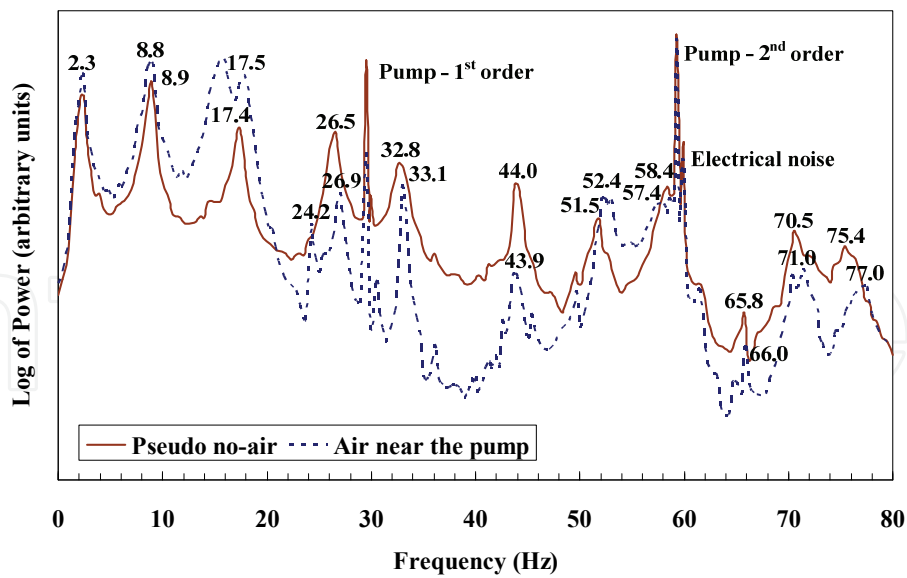


Fig. 23. The power spectra of the flow noise; data are from (Schohl, 1987a).

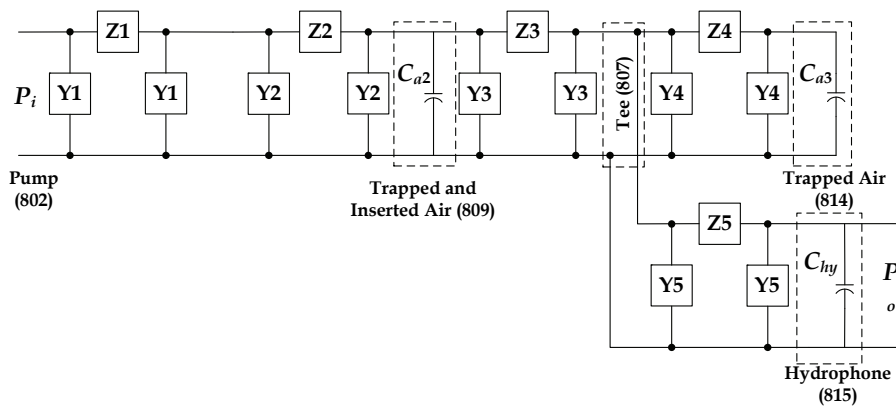


Fig. 24. Five-segment equivalent pi circuit model for the Kingston plant raw water pressure sensing line under the pseudo no-air condition.

Peak	Resonant Frequency (Hz)		
	Measured	Simulated	Difference
1	2.3	2.3	0 %
2	8.9	8.6	-3.4 %
3	17.4	17.1	-1.7 %
4	26.5	26.6	+0.4 %
5	32.8	32.0	-2.4 %
6	44.0	43.4	-1.4 %
7	51.5	51.5	0 %
8	58.4	57.8	-1.0 %
9	65.8	65.6	-0.3 %
10	70.5	70.7	+0.3 %
11	75.4	75.9	+0.7 %

Table 3. Comparison of pseudo no-air measured and simulated resonant frequencies

Table 3 shows an average absolute difference of 1.1% between the resonant frequencies of the measured data and the model with trapped air under the pseudo no-air situation, thereby verifying the model. To realize the air near the pump, another air capacitor equivalent to a 14.2 cm³ air pocket is inserted at location 812 as shown in Fig. 25. The simulation results based on the developed models are presented in Fig. 26. Comparing Figs. 23 and 26, it can be observed that the simulation results and the measured data still have good agreement after the air is inserted into the sensing line.

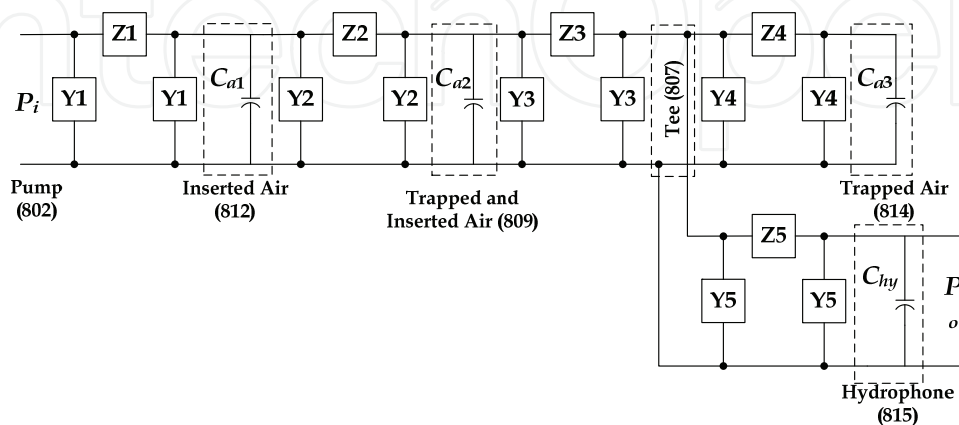


Fig. 25. Five-segment equivalent pi circuit model for the Kingston plant raw water pressure sensing line with an air pocket inserted near the pump (Lin & Holbert, 2010).

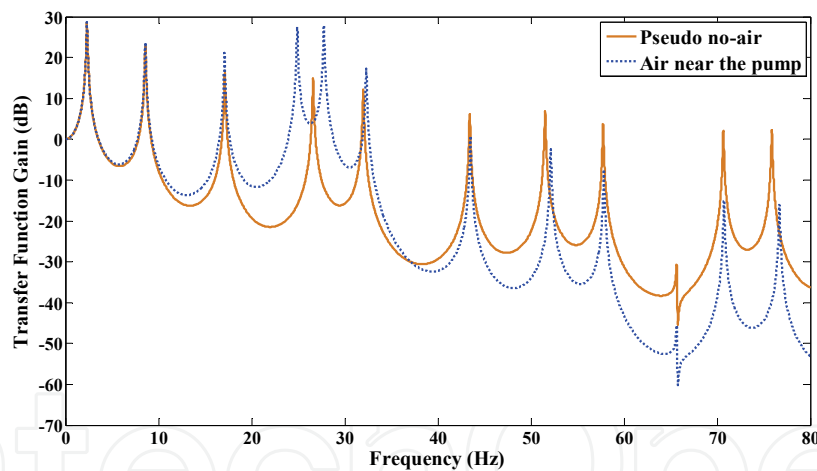


Fig. 26. Transfer functions of the Kingston steam plant raw water pressure sensing system based on the developed pressure system model.

6. Conclusions and Future Work

This chapter has detailed the establishment of online condition monitoring methods for pressure sensing systems. Each anomaly is uniquely represented by electrical equivalents, in particular:

- blockage – modified resistance, inductance, and capacitance,
- voids – additional parallel capacitance, and
- leakage – additional parallel resistance.

Models of blockage, voids, and leakage associated with instrument lines based on their electrical representations in conjunction with analyses of the operational data from a NPP

and field test measurements from an operating fossil power plant are presented. The operational data and field test measurement analysis results demonstrate behaviour consistent with the simulation results, and thereby validate the developed models.

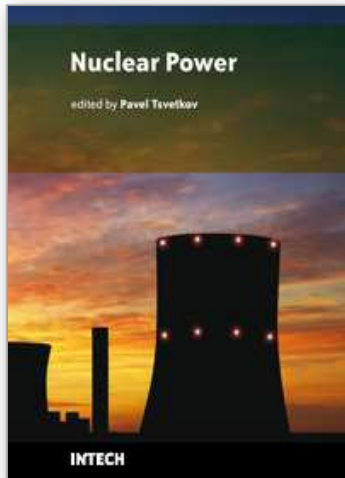
Future research for extending the work presented in this chapter could include:

- studying the situation when multiple anomaly types occur in the sensing system,
- developing effective diagnostic indicators based on the spectral feature variations due to the presence of sensing line anomalies, and
- investigating the applicability of using the developed anomaly models for fault isolation and location.

7. References

- American Society of Mechanical Engineers (ASME) (2007). Power piping. *ASME Standard*, ASME B31.1.
- Barbero, J.; Blázquez, J. & Vela, O. (2000). Bubbles in the sensing line of nuclear power plant pressure transmitters: the shift of spectrum resonances. *Nuclear Engr. and Design*, Vol. 199, No. 3, 327-334.
- Bergh, H. & Tijdeleman, H. (1965). Theoretical and experimental results for the dynamic response of pressure measuring systems. *National Aero and Astronautical Research Institute*, Amsterdam, NLR-TR F.238.
- Blázquez, J. & Ballestrín, J. (1995). Pressure transmitter surveillance: The dominant real pole case. *Prog. in Nucl. Energy*, Vol. 29, No. 3/4, 139-145.
- Clark, C. (1985). A differential pressure transducer for the measurement of high-frequency fluctuations in liquids. *Journal of Physics: Scientific Instruments*, Vol. 18, 297-302.
- Gibson, F. W. (1970). Measurement of the effect of the air bubbles on the speed of sound in water. *Acoustical Society of America*, Vol. 48, No. 5, 1195-1197.
- Glover, J. D. & Sarma, M. S. (2000). *Power System Analysis and Design*. Brooks/Cole, CA USA.
- Gogolyuk, P.; Lysiak, V. & Grinberg, I. (2004). Mathematical modeling of a synchronous motor and centrifugal pump combination in steady state. *Proc. of the IEEE PES Power System Conference and Exposition*, 1444-1448.
- Grunberg, L. & Nissan, A. H. (1949). Mixture law for viscosity. *Nature*, Vol. 164, No. 4175, 799-800.
- Hashemian, H. M.; Mitchell, D. W.; Fain, R. E. & Petersen, K. M. (1993). Long term performance and aging characteristics of nuclear plant pressure transmitters. Report prepared for the U.S. Nuclear Regulatory Commission, NUREG/CR-5851.
- Hashemian, H. M. (2006). *Maintenance of Process Instrumentation in Nuclear Power Plants*. Springer, ISBN 978-3-540-33703-4, Berlin, Germany.
- Iberall, A. S. (1950). Attenuation of oscillatory pressures in instrument lines. *Research of the National Bureau of Standards*, Vol. 45, No. 1, 85-108.
- International Society of Automation (ISA) (1999). Nuclear safety-related instrument-sensing line piping and tubing standard for use in nuclear power plants. *ISA Standard*, ISA 67.02.01-1999.
- International Society of Automation (ISA) (2005). Fossil fuel power plant instrument piping installation. *ISA Standard*, ISA 77.70-1994 (R2005).
- Izquierdo, J.; Pérez, R. & Iglesias, P. L. (2004). Mathematical models and methods in the water industry. *Mathematical and Computer Modelling*, Vol. 39, No. 11/12, 1353-1374.

- Izquierdo, J. & Iglesias, P. L. (2002). Mathematical modeling of hydraulic transients in simple systems. *Mathematical and Computer Modelling*, Vol. 35, No. 7/8, 801-812.
- Kafesaki, M.; Penciu, R. S. & Economou, E. N. (2000). Air bubbles in water: A strongly multiple scattering medium for acoustic wave. *The American Physical Society*, Vol. 84, No. 26, 6050-6053.
- Landua, L. D. & Lifshitz, E. M. (1959). *Fluid Mechanics*, Addison-Wesley, London.
- Lee, P. J.; Vítkovský, J. P.; Lambert, M. F.; Simpson, A. R. & Liggett, J. A. (2005). Leak location using the pattern of the frequency response diagram in pipelines: a numerical study. *Journal of Sound and Vibration*, Vol. 284, No. 3-5, 1051-1073.
- Lee, P.J.; Lambert, M. F.; Simpson, A. R.; Vítkovský, J. P. & Liggett, J. (2006). Experimental verification of the frequency response method for pipeline leak detection. *Journal of Hydraulic Research*, Vol. 44, No. 5, 693-707.
- Lin, K. & Holbert, K. E. (2009a). Applying the equivalent pi circuit to the modeling of hydraulic pressurized lines. *Mathematics and Computers in Simulation*, Vol. 79, No. 7, 2064-2075.
- Lin, K. & Holbert, K. E. (2009b). Blockage diagnostics for nuclear power plant pressure transmitter sensing lines. *Nuclear Engineering and Design*, Vol. 239, No. 2, 365-372.
- Lin, K. & Holbert, K. E. (2010). Void diagnostics in liquid-filled pressure sensing lines. *Progress in Nuclear Energy*, Vol. 52, No. 5, 503-511.
- Matko, D.; Geiger, G. & Gregoritz, W. (2000). Pipeline simulation techniques. *Mathematics and Computers in Simulation*, Vol. 52, No. 3, 211-230.
- Matko, D. & Geiger, G. (2002). Models of pipelines in transient mode. *Mathematical and Computer Modelling of Dynamical Systems*, Vol. 8, No. 1, 117-136.
- Müllens, J. A. & Thie, J. A. (1989). Pressure noise in pressurized water reactors. *U.S. Nuclear Regulatory Commission*, NUREG/CR-5383.
- Olson, H. F. (1957). *Acoustical Engineering*, D. Van Nostrand Co., ISBN 0193007045, Princeton.
- Schohl, G. A. (1987a). Tests at Kingston Plant of Techniques for Void Detection in Sensing Lines, Tennessee Valley Authority Report WR28-1-670-100.
- Schohl, G. A. (1987b). Additional Test and Analysis of Techniques for Air Detection in Sensing Lines, Tennessee Valley Authority Report WR28-1-670-102.
- Schohl, G. A.; Vigander, S. & Kuzniak, W. C. (1987). Detection of air in sensing lines from standing wave frequencies, *Transactions of the American Nuclear Society*, Vol. 55, 720-721.
- Schohl, G. A. & Vigander, S. (1989). Air detector for liquid-filled sensing lines. U.S. Patent, no. 4,858,460.
- Schönfeld, J. C. (1954). Analogy of hydraulic, mechanical, acoustic and electric systems. *Applied Scientific Research B*, Vol. 3, No. 1, 417-450.
- Sherstyuk, A. N. (2000). Speed of sound in a homogeneous liquid-air mixture. *Chemical and Petroleum Engineering*, Vol. 36, Nos. 5-6, 363-366.
- Sullivan, G. P.; Pugh, R.; Melendez, A. P. & Hunt, W. D. (2004). Operations & Maintenance Best Practices, A guide to achieving operational efficiency, Release 2.0, U.S. Department of Energy, Federal Energy Management Program.
- Thie, J.A. (1981). *Power Reactor Noise*. American Nuclear Society, ISBN 0-89448-025-1, La Grange Park, Illinois.
- Tyree, M. T. & Ewers, F. W. (1991). The hydraulic architecture of trees and other woody plants. *New Phytologist*, Vol. 119, No. 3, 345-360.
- Westerhof, N. et al. (1969). Analog studies of the human systemic arterial tree. *Journal of Biomechanics*, Vol. 2, No. 2, 121-143.



Nuclear Power

Edited by Pavel Tsvetkov

ISBN 978-953-307-110-7

Hard cover, 388 pages

Publisher Sciyo

Published online 17, August, 2010

Published in print edition August, 2010

The world of the twenty first century is an energy consuming society. Due to increasing population and living standards, each year the world requires more energy and new efficient systems for delivering it. Furthermore, the new systems must be inherently safe and environmentally benign. These realities of today's world are among the reasons that lead to serious interest in deploying nuclear power as a sustainable energy source. Today's nuclear reactors are safe and highly efficient energy systems that offer electricity and a multitude of co-generation energy products ranging from potable water to heat for industrial applications. The goal of the book is to show the current state-of-the-art in the covered technical areas as well as to demonstrate how general engineering principles and methods can be applied to nuclear power systems.

How to reference

In order to correctly reference this scholarly work, feel free to copy and paste the following:

Kang Lin and Keith Holbert (2010). Pressure Sensing Line Diagnostics in Nuclear Power Plants, Nuclear Power, Pavel Tsvetkov (Ed.), ISBN: 978-953-307-110-7, InTech, Available from:

<http://www.intechopen.com/books/nuclear-power/pressure-sensing-line-diagnostics-in-nuclear-power-plants>

INTECH

open science | open minds

InTech Europe

University Campus STeP Ri
Slavka Krautzeka 83/A
51000 Rijeka, Croatia
Phone: +385 (51) 770 447
Fax: +385 (51) 686 166
www.intechopen.com

InTech China

Unit 405, Office Block, Hotel Equatorial Shanghai
No.65, Yan An Road (West), Shanghai, 200040, China
中国上海市延安西路65号上海国际贵都大饭店办公楼405单元
Phone: +86-21-62489820
Fax: +86-21-62489821

© 2010 The Author(s). Licensee IntechOpen. This chapter is distributed under the terms of the [Creative Commons Attribution-NonCommercial-ShareAlike-3.0 License](#), which permits use, distribution and reproduction for non-commercial purposes, provided the original is properly cited and derivative works building on this content are distributed under the same license.

IntechOpen

IntechOpen